1 Low Energy Neutrino Scattering Overview
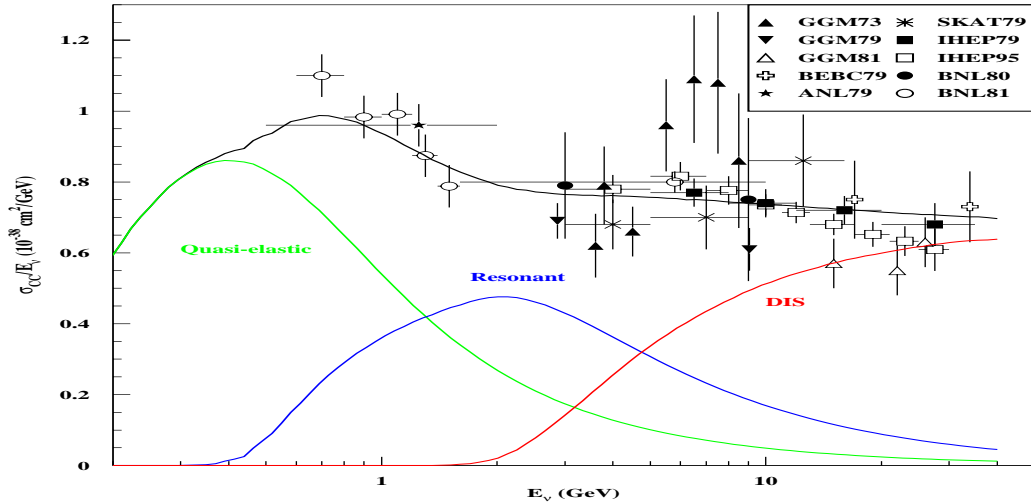

Figure 1: Total neutrino and antinuetrino cross sections (devided by energy) versus energy compared to the sum of quasielastic, resonance, and inelastic contributions (from D. Casper, Private Communication)

There are several formalisms used to discuss electron-nucleon and neutrino-nucleon (CC and NC) scattering, and the corresponding reactions on nuclear targets.

Inclusive lepton scattering can be described in either structure function language or in terms of form factors for the production of resonant final states. The two descriptions are equivalent and there are expressions that relate form factors to structure functions. In electron scattering, the vector form factors can be related to the two structure functions W_1 and W_2 (which are different for neutrons and protons) or equivalently F_2 and R.

In neutrino scattering, there are three structure functions W_1, W_2 and W_3 (or F_2, R and xF_3), which are different for the scattering from neutrons and protons, and contain both a vector and an axial vector component. In addition, because of the finite mass of the final state muon, there are additional structure functions (which are only important at very low energies) which are depend on the muon mass. These muon mass dependent structure functions can be related to the other structure functions within the framework of theoretical models.

From CVC, the vector structure functions (or form factors) measured in electron scattering can be related to the corresponding vector structure functions in neutrino scattering for specific isospin final states. For elastic scattering from spin 1/2 quarks or spin 1/2 nucleons, these relationships for the vectro form

factors are simpler. For production of higher spin resonances, the relations are more complicated and involve Clebsch-Gordon coefficients.

In contrast, the axial structure functions in neutrino scattrering cannot be related to electron scattering, except in certain limits. For example, within a quark parton model at high energies with V=A. At low Q^2, the axial and vector form factors are different, e.g. because of the differnet interactions with the pion cloud around the nucleon.

Another difference is the issue of nuclear effects in inclusive neutrino versus electron scattering. The nuclear effects can be different for axial and vector parts of the scattering (e.g. shadowing effects). They can also be different for the various structure functions (e.g. different for valence and sea quarks).

There are several theoretical constraints and sum rules that can be tested in electron and neutrino reactions (or equivalently included as a constraint in the overall anlaysis of data. Sum of the sum rules and constraints are valid at all values of Q2, and some are only valid in certain limits. These include: (a) The adler sum rules, which are separate sum rules for the axial and vector parts of W_1, and W_2, and for W_3 and are valid at all values of Q^2 (since they are based on current algebra considerations). At high Q^2, these sum rules are equivalent to the statement that the number of u valence quarks in the proton minus the number of d valence quarks is equal to 1. Other sum rules such as the momentum sum rule (sum of the momentum carried by quark and gluons is 1) and the Gross-LLewelyn-Smith sum Rule (number of valence quarks is equal to 3) have QCD corrections and break down at very low Q^2.

At very low Q^2, there is the constraint that the vector structure functions are related to the photoproduction cross section. At high Q^2 it is expected that the structure functions are described by QCD and satisfy QCD sum rules.

Quasielastic scattering(QE), resonance production, and inelastic scattering are all important components of neutrino scattering at low energies. We should clarify that the neutrino community uses the term 'quasielastic' to describe a charged-current process in which a neutrino interacts with a nucleon and produces a muon (or an electron) in the final state. The nucleon can be a free nucleon or a nucleon bound in the nucleus. The term 'quasielastic' refers to the fact that the initial state neutrino changes into a different lepton, and there is a single recoil nucleon in the final state (which changes its charge state). In contrast, the electron scattering community refers to the case of electron-nucleon scattering with a single recoil nucleon as 'elastic' scattering. The term 'quasielastic' scattering is used by the electron scattering community to describe elastic electron-nucleon scattering from bound nucleons in a nucleus. Here the term 'quasielastic' refers to the fact that the bound nucleon is quasi-free. Both of these interpertations are used in the literature.

In order to describe specific final states, one either uses the langauge of structure functions, followed by fragmentation functions at high values of Q2. At low values of Q2, many experiments describe the cross sections for specific exclusive final states. Both of these pictures need to be modified when the scattering takes place on a complex nucleus.

Figures1 (a) and (b) show the total neutrino and antineutrino cross section

(per nucleon for an isoscalar target) versus energy (at low energies) compared to the sum of quasielastic, resonance, and inelastic contributions. The sum is constructed to be continuous in W as follows. For $W > 2\ GeV$ the Bodek-Yang model is used with the axial structure functions calculated with $Z = 0.5$. The Rein-Sehgal model is used used for $W < 2\ GeV$. In addition, a fraction of the Bodek-Yang cross section is added to the Rein-Sehgal cross section between $W = 1.7\ GeV$ and $W = 2\ GeV$. The fraction increases linearly with W from 0 to 0.38 between W=1.7 and 2 W=2 GeV. These two figures also show the various contributions to the neutrino and antineutrino total cross-sections that are investigated in this proposal.

2   Quasielatic charged-current scattering

Quasielastic scatteing is discussed in detail in two recent papers by Budd, Bodek and Arrington [2]. Here we give a brief summary of the results of these two papers.

2.1   Total Quasielastic Cross Sections

Figures 2, and 3 show the QE cross section for ν and $\overline{\nu}$ with BBA-2003 Form Factors and M_A=1.00 GeV. The normalization uncertainty in the data is approximately 10%. The solid curve uses no nuclear correction, while the dashed curve [29] uses a NUANCE [32] calculation of a Smith and Moniz [30] based Fermi gas model for carbon.

This nuclear model includes Pauli blocking (see Figure 12) and Fermi motion, but not final state interactions. The Fermi gas model was run with a 25 MeV binding energy and 220 MeV Fermi momentum. The dotted curve is the prediction for Carbon including both Fermi gas Pauli blocking, and the effect of nuclear binding on the nucleon form factors as modeled by Tsushima *et al* [33] (see Figure 13). Note that this model is only valid for Q^2 less than 1 GeV^2, and that the binding effects on the form factors are expected to be very small at higher Q^2. Both the Pauli blocking and the nuclear modifications to bound nucleon form factors reduce the cross section relative to the cross section with free nucleons.

The MINERvA experiment will be able to measure these quasielastic cross sections with much greater precision. In addition, for the first time, precision measurements of the axial form factors of the nucleon for Q^2 greater than 1 GeV^2 will be done. At lower values of Q^2, where the nuclear corrections on Carbon are larger the qausielastic axial form factor is rather well known from neutrino experiments on deuterium. Here, the contribution of MINERvA will focus on understanding the nuclear effects at low Q^2 (which give the largest contribution to the integrated quasielastic cross section).
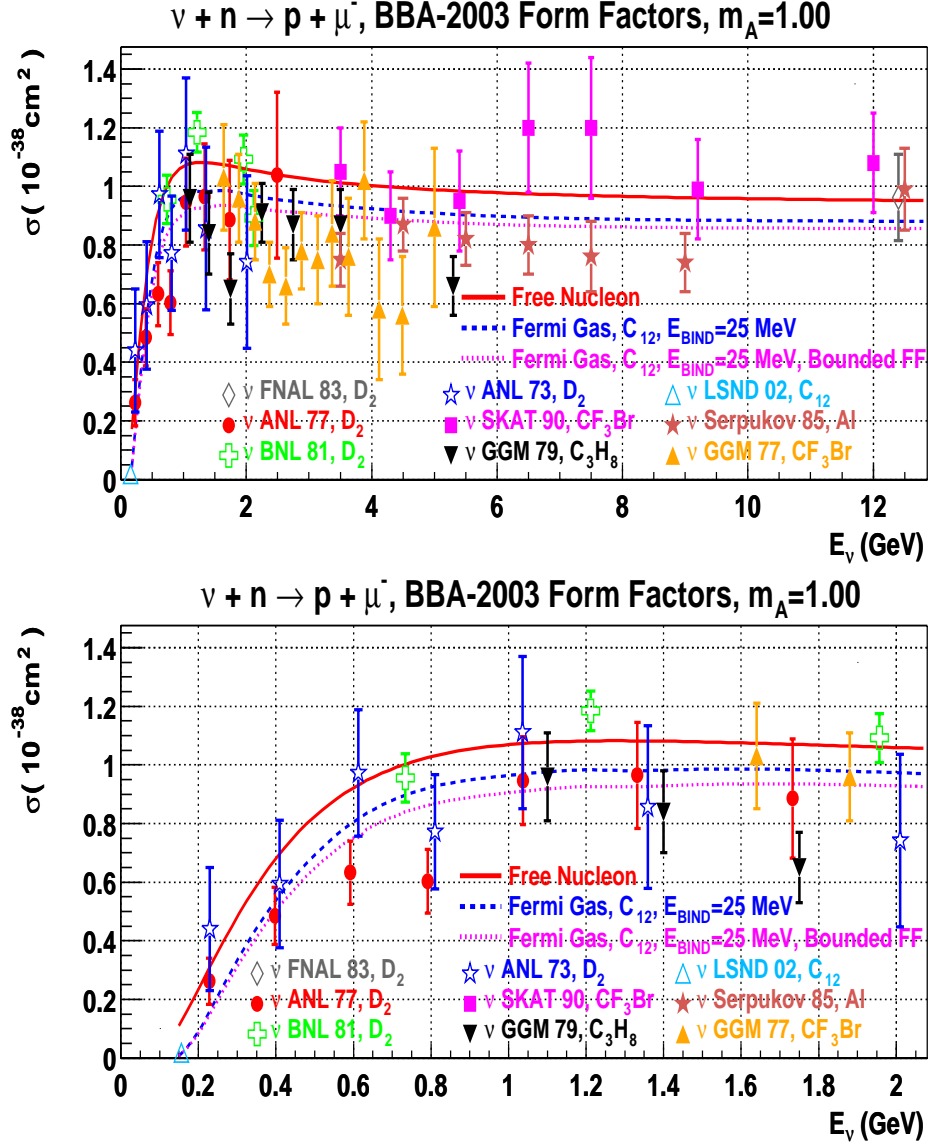
Figure 2: The QE neutrino cross section along with data from various experiments. The calculation uses M_A=1.00 GeV, g_A=−1.267, M_V^2=0.71 GeV^2 and BBA-2003 Form Factors. The solid curve uses no nuclear correction, while the dashed curve [29] uses a Fermi gas model for carbon with a 25 MeV binding energy and 220 Fermi momentum. The dotted curve is the prediction for Carbon including both Fermi gas Pauli blocking and the effect of nuclear binding on the nucleon form factors [33]. The lower plot is identical to the upper plot with the E_ν axis limit changed to 2 GeV. The data shown are from FNAL 1983 [17], ANL 1977 [15], BNL 1981 [14], ANL 1973 [22], SKAT 1990 [23], GGM 1979 [24], LSND 2002 [25], Serpukov 1985 [26], and GGM 1977 [27].
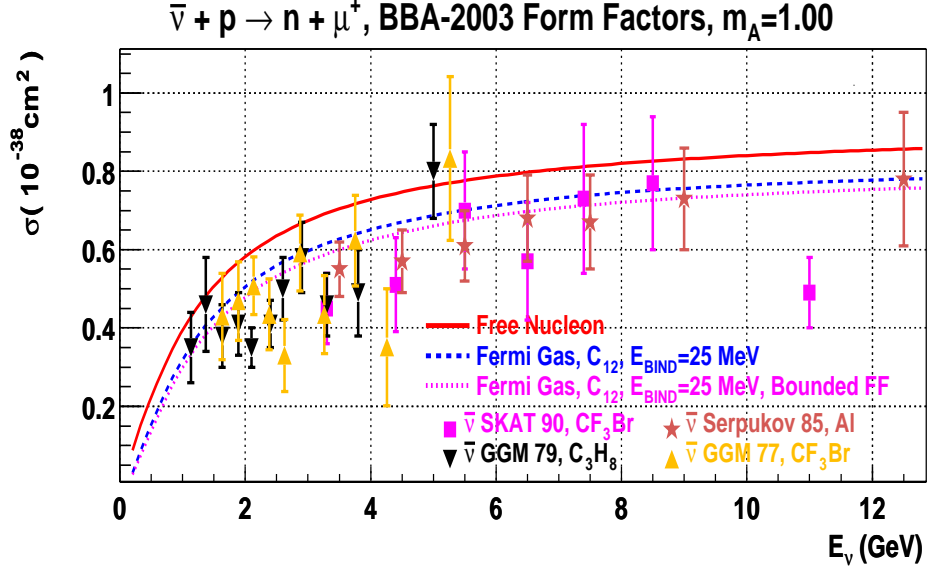
4

Figure 3: The QE antineutrino cross section along with data from various experiments. The calculation uses M_A=1.00 GeV, g_A=-1.267, M_V^2=0.71 GeV^2 and BBA-2003 Form Factors. The solid curve uses no nuclear correction, while the dashed curve [29] uses a Fermi gas model for carbon with a 25 MeV binding energy and 220 MeV Fermi momentum. The dotted curve is the prediction for Carbon including both Fermi gas Pauli blocking and the effect of nuclear binding on the nucleon form factors [33]. The data shown are from SKAT 1990 [23], GGM 1979 [28], Serpukov 1985 [26], and GGM 1977 [27].

2.1.1   Input from Electron Scattering Experiments

Recent experiments at SLAC and Jefferson Lab (JLab) have given precise measurements of the vector electromagnetic form factors for the proton and neutron. These form factors can be related to the form factors for QE neutrino scattering by conserved vector current hypothesis, CVC. These more recent form factors can be used to give better predictions for QE neutrino scattering.

The hadronic current for QE neutrino scattering is given by [3]

$$< p(p_2)|J_\lambda^+|n(p_1) >=$$
$$\overline{u}(p_2) \left[\gamma_\lambda F_V^1(q^2) + \frac{i\sigma_{\lambda\nu}q^\nu \xi F_V^2(q^2)}{2M} + \gamma_\lambda\gamma_5 F_A(q^2) + \frac{q_\lambda\gamma_5 F_P(q^2)}{M} \right] u(p_1),$$

where $q = k_\nu - k_\mu$, $\xi = (\mu_p - 1) - \mu_n$, and $M = (m_p + m_n)/2$. Here, μ_p and μ_n are the proton and neutron magnetic moments. We assume that there are no second class currents, so the scalar form factor F_V^3 and the tensor form factor F_A^3 need not be included. Using the above current, the cross section is

g_A	-1.267
G_F	1.1803×10^{-5} GeV^{-2}
$\cos\theta_c$	0.9740
μ_p	2.793 μ_N
μ_n	-1.913 μ_N
ξ	3.706 μ_N
M_V^2	0.71 GeV^2
M_A	1.00 GeV

Table 1: The most recent values of the parameters used in the 'BBA-2003' calculations.

$$\frac{d\sigma^{\nu,\,\bar{\nu}}}{dq^2} = \frac{M^2 G_F^2 cos^2\theta_c}{8\pi E_\nu^2} \times \left[A(q^2) \mp \frac{(s-u)B(q^2)}{M^2} + \frac{C(q^2)(s-u)^2}{M^4} \right],$$

where

$$A(q^2) = \frac{m^2 - q^2}{4M^2} \left[\left(4 - \frac{q^2}{M^2} \right) |F_A|^2 \right.$$
$$\left. - \left(4 + \frac{q^2}{M^2} \right) |F_V^1|^2 - \frac{q^2}{M^2} |\xi F_V^2|^2 \left(1 + \frac{q^2}{4M^2} \right) - \frac{4q^2 \, Re F_V^{1*} \xi F_V^2}{M^2} \right],$$

$$B(q^2) = -\frac{q^2}{M^2} Re F_A^*(F_V^1 + \xi F_V^2), \quad C(q^2) = \frac{1}{4} \left(|F_A|^2 + |F_V^1|^2 - \frac{q^2}{M^2} \left| \frac{\xi F_V^2}{2} \right|^2 \right).$$

Here

$$q^2 = q_0^2 - \vec{q}_3^2 = -4E_0 E' \sin^2 \frac{\theta}{2} = -Q^2 .$$

Although we have have not shown terms of order $(m_l/M)^2$, and terms including $F_P(q^2)$ (which is multiplied by $(m_l/M)^2$), these terms are included in our calculations [3].) The form factors $F_V^1(q^2)$ and $\xi F_V^2(q^2)$ are given by:

$$F_V^1(q^2) = \frac{G_E^V(q^2) - \frac{q^2}{4M^2} G_M^V(q^2)}{1 - \frac{q^2}{4M^2}}, \quad \xi F_V^2(q^2) = \frac{G_M^V(q^2) - G_E^V(q^2)}{1 - \frac{q^2}{4M^2}}.$$

We use the CVC to determine $G_E^V(q^2)$ and $G_M^V(q^2)$ from the electron scattering form factors $G_E^p(q^2)$, $G_E^n(q^2)$, $G_M^p(q^2)$, and $G_M^n(q^2)$:

$$G_E^V(q^2) = G_E^p(q^2) - G_E^n(q^2), \quad G_M^V(q^2) = G_M^p(q^2) - G_M^n(q^2).$$

The axial form factor F_A and the pseudoscalar form factor F_P (related to F_A by PCAC) are given by

$$F_A(q^2) = \frac{g_A}{\left(1 - \frac{q^2}{M_A^2} \right)^2}, \quad F_P(q^2) = \frac{2M^2 F_A(q^2)}{M_\pi^2 - q^2}.$$

6

In the expression for the cross section, $F_P(q^2)$ is multiplied by $(m_l/M)^2$. There-fore, in muon neutrino interactions, this effect is very small except at very low energy, below 0.2 GeV. $F_A(q^2)$ needs to be extracted from QE neutrino scattering. At low Q^2, $F_A(q^2)$ can also be extracted from pion electroproduction data.

For later use in Adler sum rule, we express the following functions used by Adler[4] in the notation of C.H. Llewellyn Smith [3] (which we use here).

$$|F_V(q^2)|^2 = |F_V^1(q^2)|^2 - \frac{q^2}{M^2}\left|\frac{\xi F_V^2(q^2)}{2}\right|^2$$

$$g_V(q^2) = F_V^1(q^2) + \xi F_V^2(q^2)$$

Note that $F_A(q^2)$ in our notation is the same as $g_A(q^2)$ as defined by Adler, and $F_P(q^2)$ in our notation is the same as $h_A(q^2)/M$ as defined by Adler. Also, Adler defines q^2 as positive, while we define q^2 as negative and Q^2 as positive.

Previously, people have assumed that the vector form factors are described by the dipole approximation.

$$G_D(q^2) = \frac{1}{\left(1 - \frac{q^2}{M_V^2}\right)^2}, \quad M_V^2 = 0.71\ GeV^2$$

$$G_E^p = G_D(q^2), \quad G_E^n = 0, \quad G_M^p = \mu_p G_D(q^2), \quad G_M^n = \mu_n G_D(q^2).$$

Note that G_E^p, G_M^p, and G_E^n are positive, while G_M^n and the axial form factor F_A are negative.

We refer to the above combination of form factors as 'Dipole Form Factors'. It is an approximation that has been improved by Budd, Bodek and Arington [2]. Here we use the updated form factors to which we refer as 'BBA-2003 Form Factors' (Budd, Bodek, Arrington) which are described below. Previous neutrino experiments used $g_A=-1.23$, while the best current value is -1.267. The previous world average value from neutrino experiments for M_A was 1.026 $\pm$ 0.020 GeV [6]. The value of M_A extracted from neutrino experiments depends on both the value of g_A and the values of the electromagnetic form factors which are assumed in the extraction process. Here we use the updated value [2] of M_A 1.00 $\pm$ 0.020 GeV, which has been re-extracted from previous neutrino data using the better known values for g_A and the updated 'BBA-2003' vector form factors. This value of M_A is in good agreement with the theoretically corrected value from pion electroproduction [6] of 1.014 $\pm$ 0.016 GeV.

Figure 8 shows the 'BBA-2003' fits to $\mu_p G_E^p/G_M^p$. Note that at present there is a discrepancy between two different ways of measuring the ratio of electric and magnetic form factor of the proton. The fit including only cross section data (i.e. using Rosenbluth separation) is roughly flat versus Q^2 ($Q^2 = -q^2$) and is consistent with form-factor scaling. This is what is expected if the electric charge and magnetization distributions in the proton are the same. However, the new technique of polarization tranfer yields a much lower ratio at high
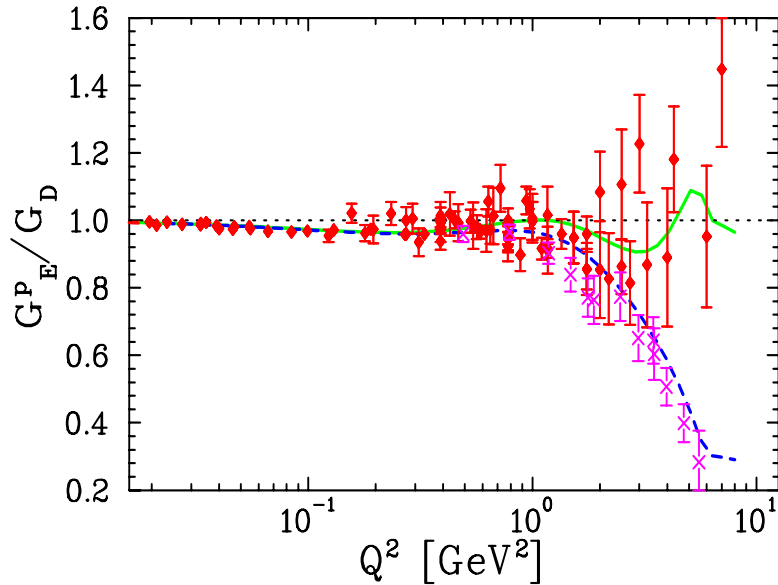
7

Figure 4: Fits to G_E^p/G_D, using cross section data only (solid), compared with 'BBA-2003' combined fits to both the cross section and polarization transfer data (dashed). The diamonds are the from Rosenbluth extractions and the crosses are the Hall A polarization transfer data. Note that the fit is to cross sections, rather than fitting directly to the extracted values of G_E^p shown here. Since the difference between the two is only at high Q^2, the two fits yield similar results for the predicted neutrino-nucleon cross sections.

Q^2, and indicates that there is a difference between the electric charge and magnetization distributions in the proton. At present the polarization transfer technique is believed to be more reliable and less senistive to radiative effects from two photon corrections.

If the electric-charge and magneization distribution in the proton are very different, then a test of the high Q^2 behavior of the axial form factor is of interest as an additional input to understand the origin of this difference. This is one of the measurementc that can be done in MINERvA. At present, there are several proposal at Jlab to further investigate this issue. In addition, there are several groups investigating two photon corrections to elastic electron scattering in order to see if the two measurements can be reconciled.

In the BBA-2003 analysis a combined fit is done, using the cross section data combined with the polarization tansfer ratio, the ratio decreases with Q^2 in the combined fit to cross section and polarization transfer data. The combined fit to both cross section and polarization transfer data is used as the default BBA-2003 form factors. Although the polarization transfer measurement is believed to have smaller systematic error, especially at high Q^2, the origin of this disagreement is not known. If this disagreement comes from radiative corrections

to the electron, in particular two-photon exchange terms, then the polarization transfer extraction will give the correct ratio, but the overall scale of G_E^p at low Q^2 would be shifted down by $\approx 3\%$. Because the fit is constrained as $Q^2 \to 0$, there will not be an overall shift in G_E^p at low Q^2, but there will be some uncertainty in the low Q^2 behavior. Current experiments at JLab aim to better understand the source of the disagreement by looking at the recoil proton in elastic electron-proton scattering, thus minimizing the sensitivity to the dominant sources of uncertainty in previous Rosenbluth separations. However, since this discrepancy is most prominent at high Q^2, and the fit is constrained at low Q^2, it has only a relatively small effect on the neutrino QE scattering cross section.

The fractional contributions of $G_M^p, G_M^n, G_E^p, G_E^n$ and F_A to the distribution in Q^2 for quasileastiv events in neutrino running and antineutrino running with the NUMI low energy beam configuration are shown in Figure 5. These contributions were determined by looking at the difference between the cross section calculated usintg BBA-2003 form factors and the cross section when each of the following form factors $G_M^p, G_M^n, G_E^p, G_E^n$ and F_A are set to zero. Because of intereference terms, the sum of the fraction does not have to add up to 1.0.
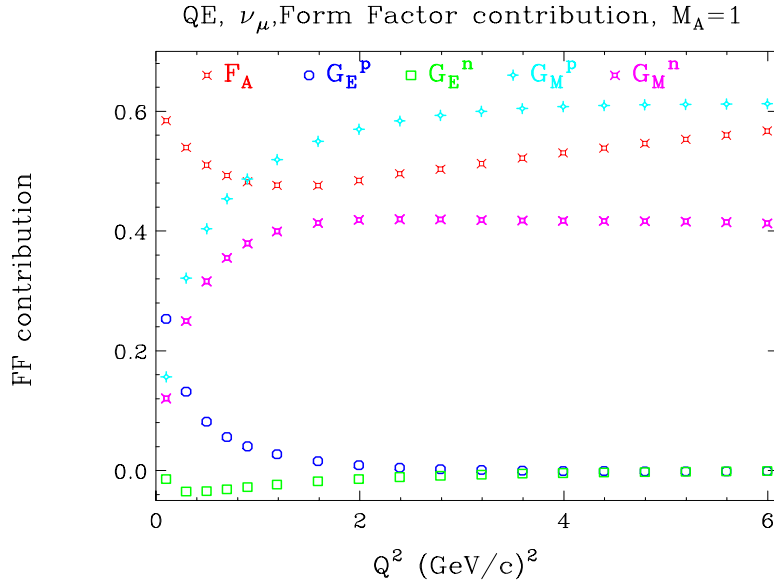

Figure 5: The fractional contributions of $G_M^p, G_M^n, G_E^p, G_E^n$ and F_A to the distribution in Q^2 for quasielastic events in neutrino (top) and antineutrino (bottom) running with the NUMI low energy beam configuration.

	data	a_2	a_4	a_6	a_8	a_{10}	a_{12}
G_E^p	CS + Pol	3.253	1.422	0.08582	0.3318	-0.09371	0.01076
G_M^p	CS + Pol	3.104	1.428	0.1112	-0.006981	0.0003705	-0.7063E-05
G_M^n		3.043	0.8548	0.6806	-0.1287	0.008912	
G_E^p	CS (test)	3.226	1.508	-0.3773	0.6109	-0.1853	0.01596
G_M^p	CS (test)	3.188	1.354	0.1511	-0.01135	0.0005330	-0.9005E-05

Table 2: The coefficients of the inverse polynomial fits for the G_E^p, G_M^p, and G_M^n. The combined fits for the proton include both the cross section data and the Hall A polarization transfer data. Note that these different polynomials replace G_D in the expression for G_E^p, G_M^p, and G_M^n. The values in this the table (CS+POL) along with the fit of G_E^n Krutov *et. al.* [12] (see text) will be referred to as 'BBA-2003 Vector Form Factors'. The CS (test) is a fit which ignores the polarization transfer data.

2.2 Input from Electron Scattering Quasielastic Scattering

Table 1 summarizes the most up to date values of the coupling constants and magnetic moments that we use in our calculations of quasielastic cross sections.

2.3 'BBA-2003' updated form factors

The 'BBA-2003' updated fit to the proton electromagnetic form factors is similar to the one described in Ref. [7], but using a slightly different fitting function (described below), and including additional data to constrain the fit at low Q^2 values. Note that in contrast to the functional form used in Ref. [8], we only include even powers of Q in our fit. This is because odd powers of Q are not theoretically allowed. For example, one can use analyticity [9, 10] to show that there are no odd terms in Q in the limit $Q \to 0$.

The vector form factors can be determined from electron scattering cross sections using the standard Rosenbluth separation technique [7], which is sensitive to radiative corrections, or from polarization measurements using the newer polarization transfer technique [11]. The polarization measurements do not directly measure the form factors, but measure the ratio G_E/G_M. Figures 4, 6, and 7 show the ratio of the fits divided by the dipole form, G_D.

To account for the fact that deviations from the dipole form are different for each of the different form factors, the electron scattering data are fit for each of the form factors to an inverse polynomial

$$G_{E,M}^N(Q^2) = \frac{G_{E,M}^N(Q^2 = 0)}{1 + a_2 Q^2 + a_4 Q^4 + a_6 Q^6 + ...}.$$

Table 2 shows the parameters of the 'BBA-2003' fit to the proton data using both cross section data together with the polarization transfer data from JLab
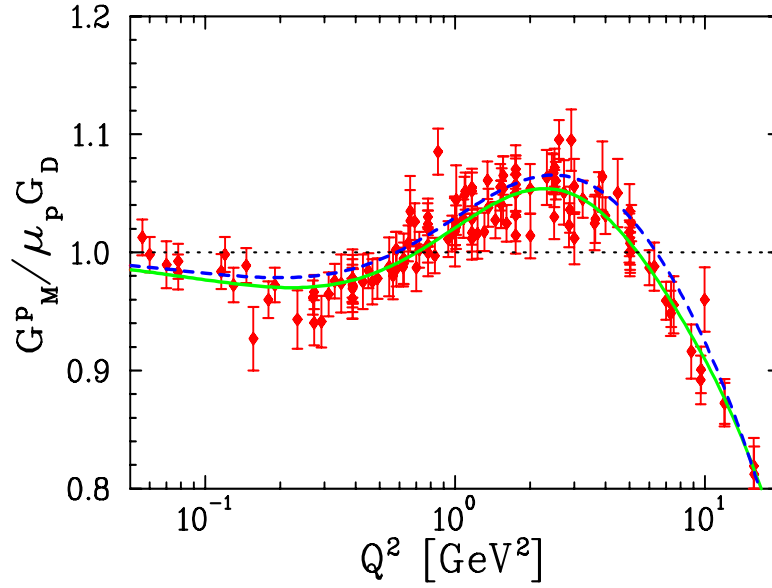
Figure 6: 'BBA-2003' fits to $G_M^p/\mu_p G_D$. The lines and symbols have the same meaning as Figure 4.
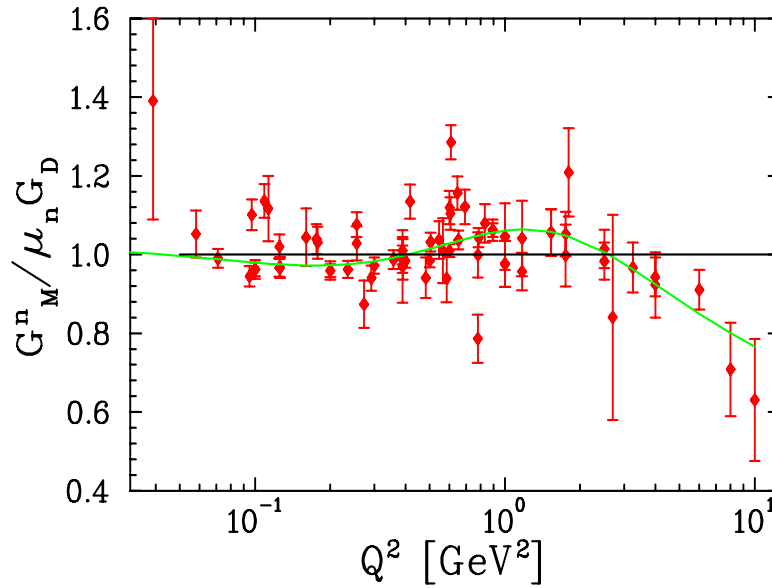

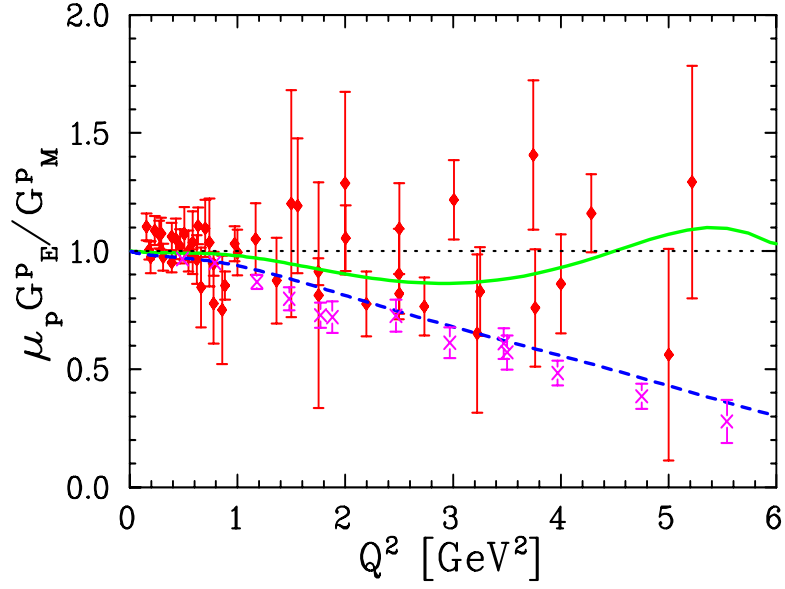Figure 7: 'BBA-2003' fit to $G_M^n/\mu_n G_D$. The lines and symbols have the same meaning as Figure 4.

Figure 8: Ratio of G_E^p to G_M^p as extracted by Rosenbluth measurements and from polarization measurements. The lines and symbols have the same meaning as Figure 4.
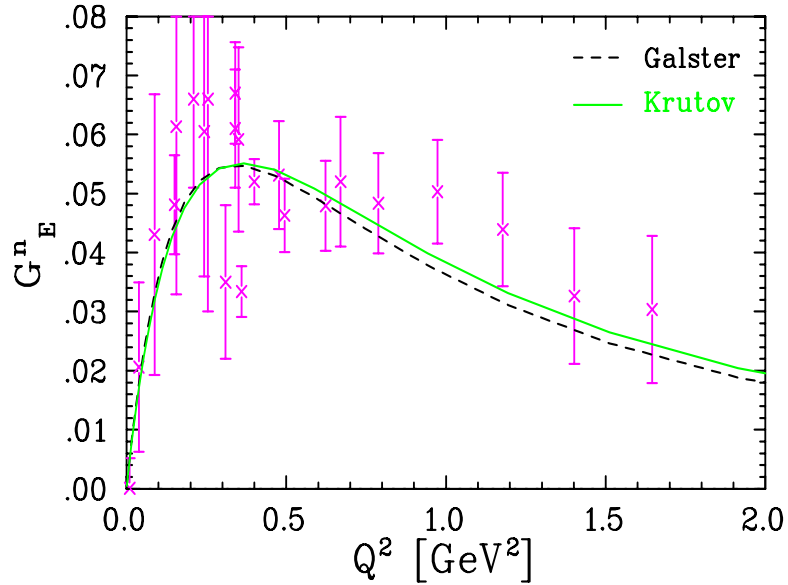

Figure 9: Data and fits to G_E^n. The dashed line is the Galster *et al.* fit [13], and the solid line is the Krutov *et al.* fit [12].
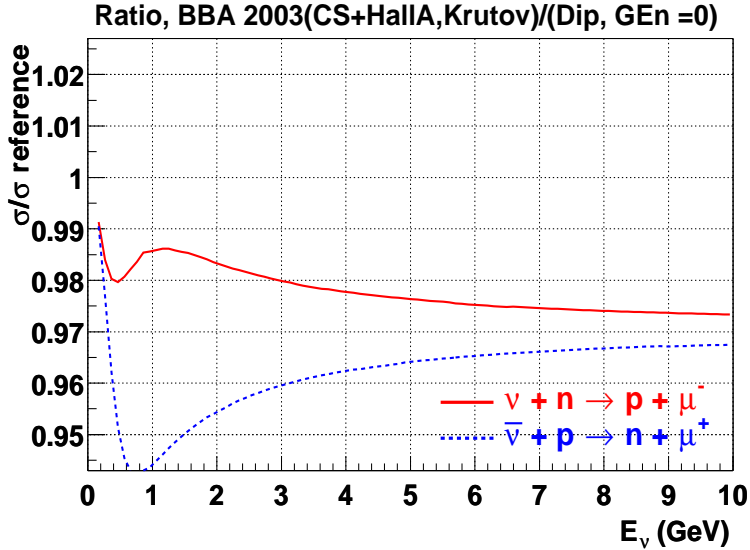
Figure 10: Ratio versus energy of predicted neutrino (antineutrino) QE cross section using BBA-2003 Form Factors to the prediction using the dipole approximation with $G_E^n=0$ (with M_A kept fixed).

Hall A. For G_E^p, the parameters in Table 2 are used for $Q^2 < 6$ GeV^2. For $Q^2 > 6$ GeV^2, the ratio of G_E^p/G_M^p is assumed to be constant:

$$G_E^p(Q^2) = G_M^p(Q^2) \frac{G_E^p(6 \text{ GeV}^2)}{G_M^p(6 \text{ GeV}^2)}$$

Since the neutron has no charge, G_E^n must be zero at $q^2=0$, and previous neutrino experiments assumed $G_E^n(q^2)=0$ for all q^2 values. However, it is non-zero away from $q^2=0$, and its slope at $q^2=0$ is known precisely from neutron-electron scattering. At intermediate Q^2, recent polarization transfer data give precise values of $G_E^n(q^2)$. Our analysis uses the parameterization of Krutov *et. al.* [12]:

$$G_E^n(Q^2) = -\mu_n \frac{a\tau}{1+b\tau} G_D(Q^2), \quad \tau = \frac{Q^2}{4M^2},$$

with $a = 0.942$ and $b = 4.61$. This parameterization is very similar to that of Galster *et al.* [13], as shown in Figure 9. The parameters in Table 2, along with the fit of G_E^n of Krutov *et. al.* [12], are referred to as 'BBA-2003 Form Factors'. For BBA-2003 Form Factors, both the cross section and polarization data are used in the extraction of G_E^p and G_M^p.

Figure 10 shows the ratio versus neutrino energy of the predicted neutrino (antineutrino) QE cross section on nucleons using the 'BBA-2003' Vector Form Factors to the prediction using the Dipole Vector Form Factors (with $G_E^n=0$

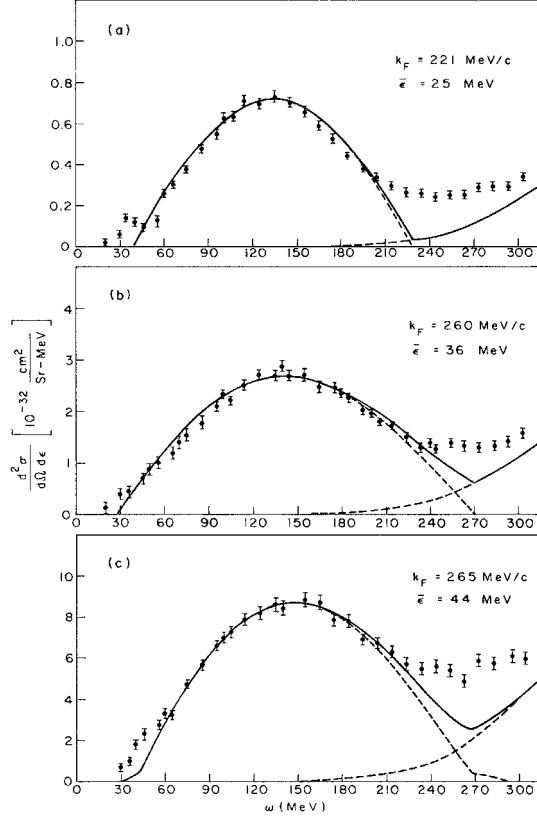and M_A kept fixed). This plot indicates that it is important to use the updated form factors.

Figure 11: Extraction of the Fermi Gas model parameters i.e. the effective K_f and nuclear potential binding energy ϵ from 500 MeV electron scattering data (from Moniz. [30]. (a)Carbon, (b) Nickel and (c) Lead

3   Nuclear Effects in Quasielastic Scattering from Bound Nucelons

There are three important effects on the inclusive quasielastic cross section on nuclear targets. These are (a) Fermi Motion, (b) Pauli Blocking and (c) Binding corrections to the nucleon form factors due to distortion of the both the nucleon size or distortions of the pion cloud around the nucleon in the nucleus. Figure 12 shows the nuclear suppression versus Q^2 from a NUANCE [32] calculation [29] of a Smith and Moniz [30] based Fermi gas model for carbon. This nuclear model includes Pauli blocking and Fermi motion (but not final state interactions). The
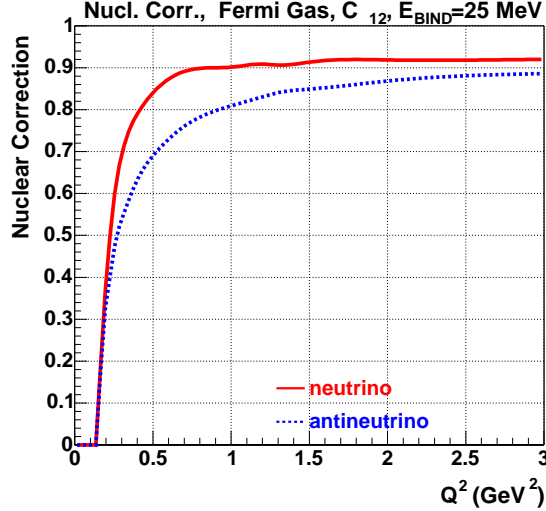
14

Figure 12: The Pauli blocking suppression for a Fermi gas model for carbon with a 25 MeV binding energy and 220 MeV Fermi momentum.

Fermi gas model was run with a 25 MeV nuclear potential binding energy ϵ and 220 MeV Fermi momentum K_f. Figure 11 from Moniz et. al. [30] shows how the effective K_f and nuclear potential binding energy ϵ (within a Fermi-gas model) for various nuclei was extracted from electron scattering data. The effective K_f is extracted from the width of the electron scattered energy, and the nuclear potential binding energy ϵ is extracted from the shifted location of the quasielastic peak. Figure 27 shows the effective K_f for various nuclear targets.

Figures 13 and 14 show the prediction for the nuclear binding effect on the nucleon form factors (i.e. the ratio of bound to free nucleon form factors for F_1, F_2, F_A) in neutrino scattering, and for the vector form factors G_E^p, G_E^n, G_M^p and G_M^n in electron scattering as modeled by Tsushima et al [33]. At low Q^2 the effect of the nuclear binding effects from this model are similar to what is observed in experiments at Jlab [10]. Both the Pauli blocking and the nuclear modifications to bound nucleon form factors reduce the cross section relative to the cross section with free nucleons. However, it is more likely that the low Q^2 deviations are not actually modifications of the actual nucleon form factors, but rather effects of interaction with the pion cloud for Q^2 less than 1 GeV^2. Note that experiments from Jlab indicate that the binding effects on the form factors are expected to be very small at higher Q^2 (as described in the next section).
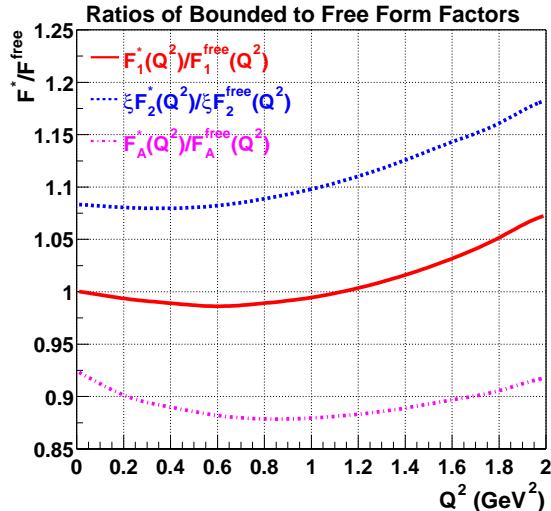
15

Ratios of Bounded to Free Form Factors

F^*/F^{free}

$F_1^*(Q^2)/F_1^{free}(Q^2)$

$\xi F_2^*(Q^2)/\xi F_2^{free}(Q^2)$

$F_A^*(Q^2)/F_A^{free}(Q^2)$

Q^2 (GeV^2)

Figure 13: The ratio of bound nucleon (in Carbon) to free nucleon form factors for F_1, F_2, and F_A from ref [33]. Note that this model is only relevant for Q^2 less than 1 GeV^2, and that the binding effects on the form factors are expected to be very small at higher Q^2. At low Q^2 the effect of the nuclear binding effects from this model are similar to what is observed in experiments at Jlab [10].

4 Detection of recoil nucleons

The calculation for the inclusive cross section assumes that only the final state muon is detected. In neutrino experiments, detection of the recoil nucleon is sometimes required in order to differentiate between quasielastic and inelastic events. Therefore, the final state interaction of the final state proton with the remaining nucleons also needs to be modeled (which leads to a reduction of the number of identified quasielastic events). Similarly, quasielastic scattering with nucleons in the high momenta region of the spectral functions also needs to be modeled. This requires more sophisticated models than the simple Fermi-Gas model. Conversely, inelastic events (such as in resonance production) may be misidentified as quasielastic events if the final state pion is absorbed in the nucleus. The best way to model these effects is to do an analysis on samples of electron scattering data on nuclear targets (including the hadronic final states) in order to test the effects of the experimental cuts on the final state nucleons. This kind of study is being planned by a Rochester group in collaboration with the Hall B CLAS collaboration. Such an investigation also tests the validity of the binding off-shell corrections to the nucleon form factors for nucleons bound in a nucleus.

Current e,e'p experiments at intermediate Q^2 are not well described by the
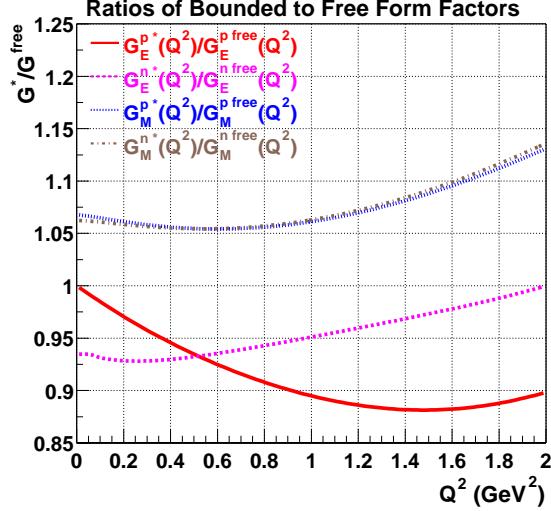
Figure 14: The ratio of bound nucleon (in Carbon) to free nucleon form factors for G_E^p, G_E^n, G_M^p and G_M^n from ref [33]. Note that this model is only relevant for Q^2 less than 1 GeV^2, and that the binding effects on the form factors are expected to be very small at higher Q^2. At low Q^2 the effect of the nuclear binding effects from this model are similar to what is observed in experiments at Jlab [10].

impulse approximation with distortion effects. One is forced to introduce a quenching factor which is large for low $Q^2 \sim 0.3$ GeV^2. This effect has been modeled by Tsushima *et al* [33] as binding corrections to nucleon form factors. However this factor cannot be strickly interpreted as a change of the form factor of the nucleus because for large Q^2 the suppression becomes much smaller and may be practically gone [10] by Q^2=2 GeV^2.

The interpertation of M. Strikman and others [10] is that one is dealing here with renormalization of the interaction of nucleons at low energy scale (natural in the Fermi liquid theory) which is essentially gone at large Q^2. What this implies for low Q^2 is basically the statement that the theory is not good enough and hence it is difficult to calculate cross section in νA scattering at low Q^2 from first principles. It is not clear how well the rescaling from e,e' to νA will work under these conditions. There may be some differences since the pion field plays a rather different rols in two cases (as can be seen from the different masses entering in the axial and vector electromagnetic form factors). Therefore, one should take the predictions of the model of Tsushima *et al* [33] only as an indication of the possible magnitude of these effects (and use it only at low Q^2). More theoretical and experimental studies are needed. MINERvA can address this question by investigating nuclear and binding effects in Carbon in

neutrino scattering, and compare the data to nuclear effects observed in electron scattering at Jlab.

One example of this is shown in figure 15 for Helium 3. The figure shows the ratio of G_M/G_E measured for nucleons bound in Helium3 (by looking at the polarization of the recoil protons) devided by the theoretical pedictions for this ration which include all known nuclear effects for two models. One model (which is valid at low Q^2) uses Optical Potentials. The other model (which is valid at higher Q^2) uses the Glauber approach. The curves labled (QMC) are the model predictions if we include the binding effects in the nucleon form factors modeled by Tsushima *et al* [33]. These data indicate that at high Q^2, there is no evidence for for nuclear binding effects in the form factors.

Polarization Transfer in ^{4}He$(\vec{e}, e'\vec{p})^3$H : results
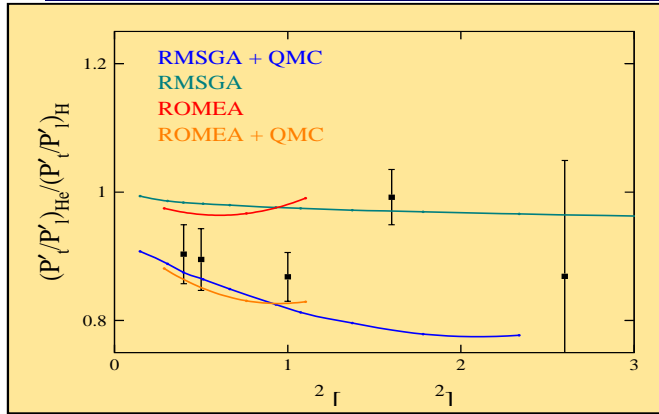
$p +^3 He$ *optical potentials : W.T.H. van Oers, PRC* **25** *(1982) 390.*
Data : S. Dieterich et al., *PLB* **500** *(2001) 47 and S. Strauch* et
al., *PRL* **91** *(2003) 0523011.*

Figure 15: The ratio of G_M/G_E measured for nucleons bound in Helium 3 (from the polarization of the recoil protons) devided by the theoretical pedictions including all known effects for two models. One model (which is valid at low Q^2) uses Optical Potentials. The other model (which is valid at higher Q^2) uses the Glauber approach. The curves labled (QMC) are the model predictions if we include the binding effects in the nucleon form factors modeled by Tsushima *et al* [33]. These data indicate that at high Q^2, there is no evidence for for nuclear binding effects in the form factors.
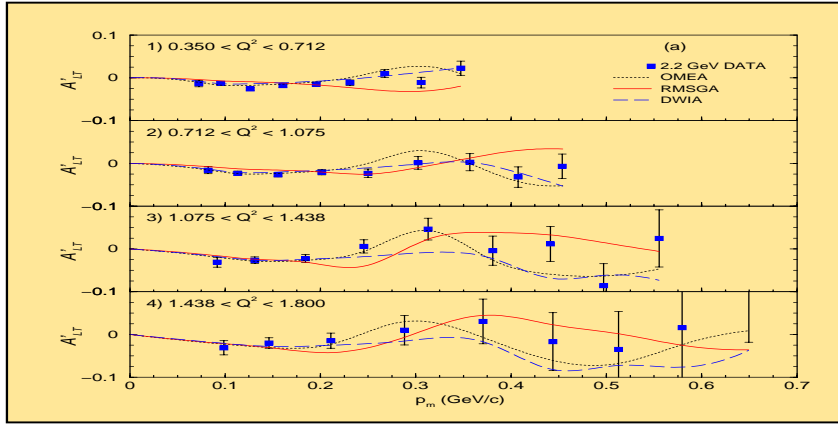
As mentioned earleir members of the Rochester MINERvA group (Steve Manly) in collaboration with Jlab (Will Brooks) will be working CLAS collaboration to study hadronic final states in electron scattering on nuclear targets using existing Jlab Hall B CLAS data. This analysis will provide information on hadronic final states in quasielastic and inelastic resonance production in electron scattering (for testing theoretical models to use in both electron and

neutrino experiments)

In addition, the we wiil be collaborating with the Ghent nuclear physics group in Belgium [35], to model both electron and neutrino quasielastic scattering on nuclei over the entire range of Q^2. This will give us the theoretical tools do a precise extraction of the axial form factor of the nucleon using our data on Carbon by performing the same analysis on neutrino and electron scattrering data in the same range of Q^2

An example of this is shown in figure 16 where the difference between electron scattering data in the quasielastic region (for Carbon) for which both the final state electron and proton are detected is compared to the prediction of theoretical models versus the momentum of the recoil proton. Extension of these models to neutrino scattering is currently under way.

Figure 16: The difference between electron scattering data in the quasielastic region (for Carbon) for which both the final state electron and proton are detected, compared to the prediction of theoretical models versus the momentum of the recoil proton. Extension of these models to neutrino scattering is currently under way.

4.1 A re-extraction of the axial form factor from previous neutrino data on deuterium

Previous neutrino measurements, mostly bubble chamber experiments on deuterium, extracted M_A using the best known assumptions at the time. Changing these assumptions changes the extracted value of M_A. Hence, M_A needs to be updated using new form factors and up-to-date couplings. Budd, Bodek and

Arrington updated the results from three previous deuterium bubble chamber experiments. These are Baker *et al.* [14], Barish *et al.* [15], Miller *et al.* [16], and Kitagaki *et al.* [17]. Barish *et al.* and Miller *et al.* are the same experiment, with the analysis of Miller *et al.* including the full data set, roughly three times the statistics included in the original analysis. On average, correcting for the various assumptions in form factors and couplings results in a decrease of 0.026 in the extracted value of M_A. This is why we use a value of 1.00 instead of the previous world average of 1.026.

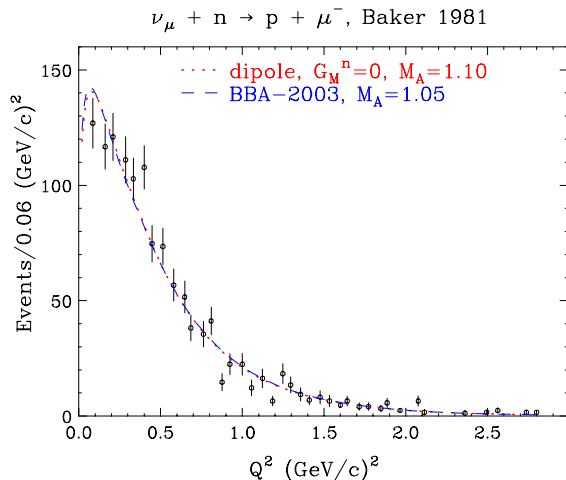$$\nu_\mu + n \to p + \mu^-, \text{ Baker 1981}$$

Figure 17: A comparison of the Q^2 distribution using 2 different sets of form factors. The data are from Baker *et al.* [14]. The dotted curve uses Dipole Form Factors with $G_E^n = 0$ and $M_A = 1.10 \ GeV$. The dashed curve uses BBA-2003 Form Factors with $M_A = 1.05 \ GeV$. The two curves cannot be distinguished from one another. This illustrates that it is important to use the most up to date information on vector form factors from electron scattering experiments when extracting the axial form factor from neutrino data.

Figure 17 shows the Q^2 distribution from the Baker *et al.* [14] neutrino experiment compared to the prediction assuming Dipole Form Factors with G_E^n=0 and M_A=1.10 GeV. Also shown are the prediction using BBA-2003 Form Factors and M_A=1.050 GeV. When we modify the electromagnetic form factors, we can use a diffeernt M_A to describe the same Q^2 distribution. Although the overall total cross sections are different, there is no modification of the Q^2 dependence when a contribution to the distribution is shifted between the electromagnetic and axial form factors. Therefore, we conclude that with the same value of g_A, the use of Dipole Form Factors (and Gen =0) instead of the BBA-2003 form factors lead to an error in extracted value of M_A of 0.050 GeV, independent of the details of the experiment.

4.2   Extractions of the axial form factor in MINERvA

Current and future high statistics neutrino experiments at low energies (such as MiniBoone, JPARC and MINERvA) use an active nuclear target such as scintillator (e.g. Carbon). As shown in Figure 18 The maximum Q^2 values that can be reached with neutrino energies of 0.5, 1.0, 1.5 and 2 GeV are 0.5, 1.2, 2,1 and 2.9 GeV^2. Since MiniBoone and JPARC energies are in the 0.7 GeV range, these experiments probes the low $Q^2 < 1 \, GeV^2$ region where nuclear effects are very large (see Figures 12 and 13) and where the axial from factor is already known very well from neutrino data on deuterium (see Figure 17). The low Q^2 ($Q^2 < 1 \, GeV^2$) MiniBoone and JPARC experiments can begin to investigate the various nuclear and binding effects in Carbon in neutrino scattering versus those observed in electron scattering at Jlab.
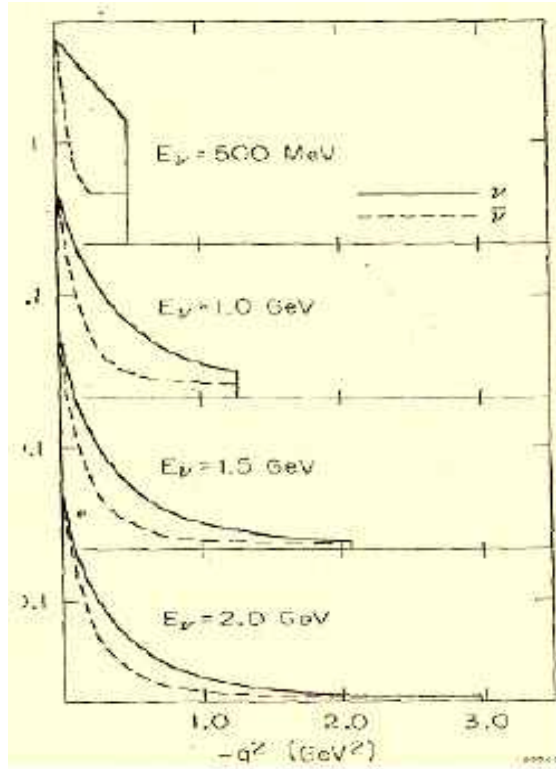

Figure 18: Q^2 distributions for different incident neutrino and antineutrino energies illustrating the maximum Q^2 reach at each energy

At higher $Q^2 \, GeV^2$, as shown by the BBA-2003 fits to the vector form factors, the dipole approximation can be as much as factor of 2 wrong for the vector form factors for $Q^2 > 2 GeV^2$. Therefore, there is no reason for this form to also be valid for the axial form factors. As can be seen from Figure 17

there is very little data for the axial form factor in the high Q^2 region (where nuclear effects are smaller). Both the low Q^2 ($Q^2 < 1\ GeV^2$) and high Q^2 ($Q^2 > 2\ GeV^2$) regions are accessible at higher energy experiments such as MINERvA at Fermilab (which can span the 2-8 GeV energy neutrino range).

Figure 19 shows the ratio of the fractional error in the differential cross section for neutrinos (a) and antineutrinos (b) versus Q^2 to the fractional error in the various form factors. As can be seen in the plot, the fractional error in the axial form factor is almost the same as the factional error in the measured differential cross section. In contast, the differential cross section at high Q^2 is not very sensitive to the values of G_E^p and G_E^n at high Q^2. This is because the fractional contribution of the electric form factors to the differential cross section in this region is small as illustrated in Figure 5.
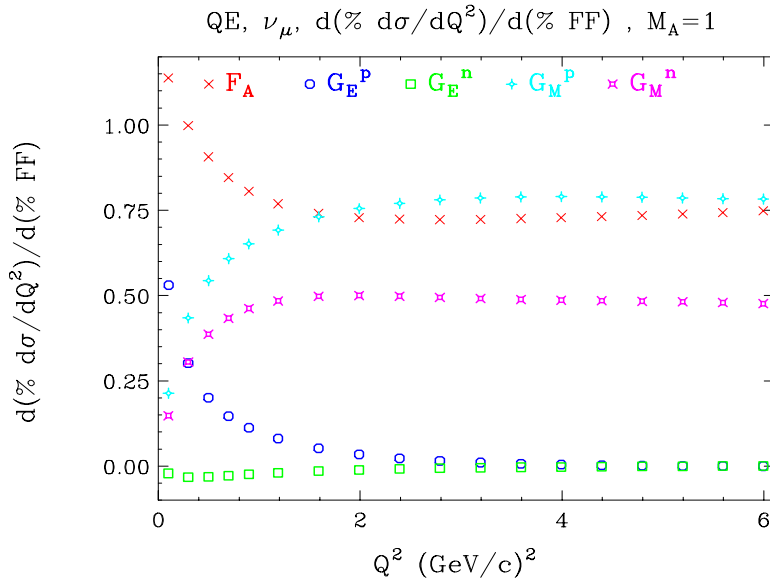

Figure 19: Ratio of the fractional error in the differential cross section versus Q^2 (for neutrinos and antineutrinos) to the fractional error in the various form factors. As can be seen in the plot, the fractional error in the axial form factor is almost the same as the factional error in the measured differential cross section.

Note that the high Q^2 region does not contribute much to the total quasielastic cross section. Therefore, it does not contribute much to the uncertainties in the total cross section. The measurement of the axial form factor in the high Q^2 region (which can be done in MINERvA) is mostly of interest in the investigation of the vector and axial structure of the nucleon.

For example, for 1 year of running in the medium energy beam (ME) and a fiducial volume of 1.4m by 1.4m by 1.4m of active scintillator the number of quasielastic events is 115,000. Figure 20 (linear) and Figure 21 (log) show the extracted values and errors of F_A from a sample of 115.000 events in the
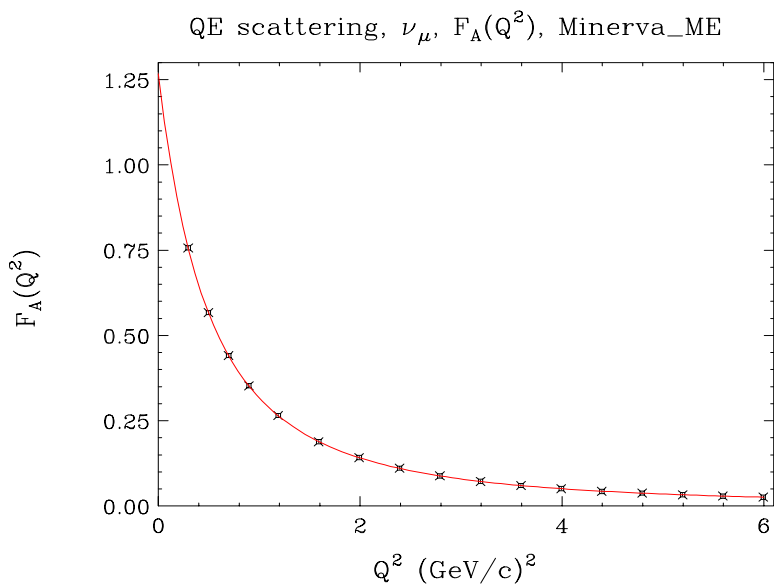
QE scattering, ν_μ, $F_A(Q^2)$, Minerva_ME

Figure 20: Linear plot (a) neutrinos and (b) antineutrinos : The extracted values and errors of F_A from a sample of quasielatic events in the MINERvA active Cargon target under the assumption that F_A is described by the dipole form factor with M_A of 1 GeV. This corresponds to a total of the currently planned 4 years of running in the Low Energy Beam Configuration.
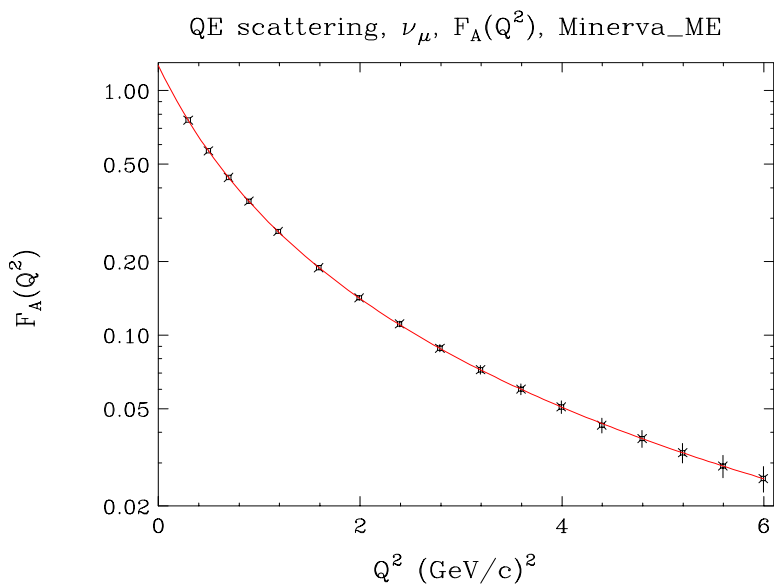
Figure 21: Logarithmic plot (a) neutrinos and (b) antineutrinos: The extracted values and errors of F_A from a sample of quasielatic events in the MINERvA active Cargon target under the assumption that F_A is described by the dipole form factor with M_A of 1 GeV. This corresponds to a total of the currently planned 4 years of running in the Low Energy Beam Configuration.
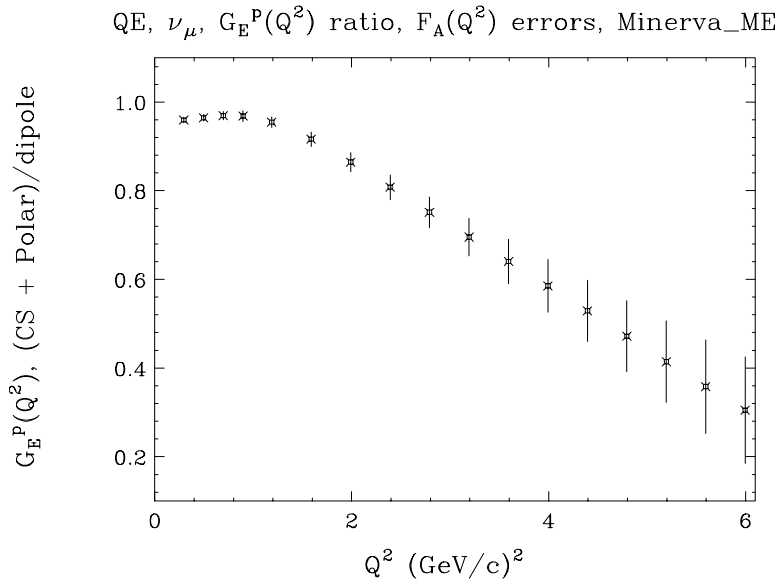
QE, ν_μ, $G_E{}^P(Q^2)$ ratio, $F_A(Q^2)$ errors, Minerva_ME

Figure 22: (a) Neutrino, (b) Antineutrino. The extracted ratio and error in F_A/F_A(Dipole) under the assumptions that this ratio is described by the ratio of G_E^p(Cross-Section+POLARIZATION)$/G_E^p$(Dipole) (which is the currently assumed form factor in the BBA2003 parametrization for G_E^p). Note a ratio of 1.0 is expected if the axial form factor is described exactly by the dipole form. This corresponds to a total of the currently planned 4 years of running in the Low Energy Beam Configuration.

QE, ν_μ, $G_E{}^P(Q^2)$ ratio, $F_A(Q^2)$ errors, Minerva_ME

Figure 23: (a) Neutrino, (b) Antineutrino.The extracted ratio and error in F_A/F_A(Dipole) under the assumptions that this ratio is described by the ratio of G_E^p(Cross-Section+POLARIZATION)$/G_E^p$(Cross-Section). Note a ratio of 1.0 is expected if the axial form factor is described exactly by the dipole form. This corresponds to a total of the currently planned 4 years of running in the Low Energy Beam Configuration.
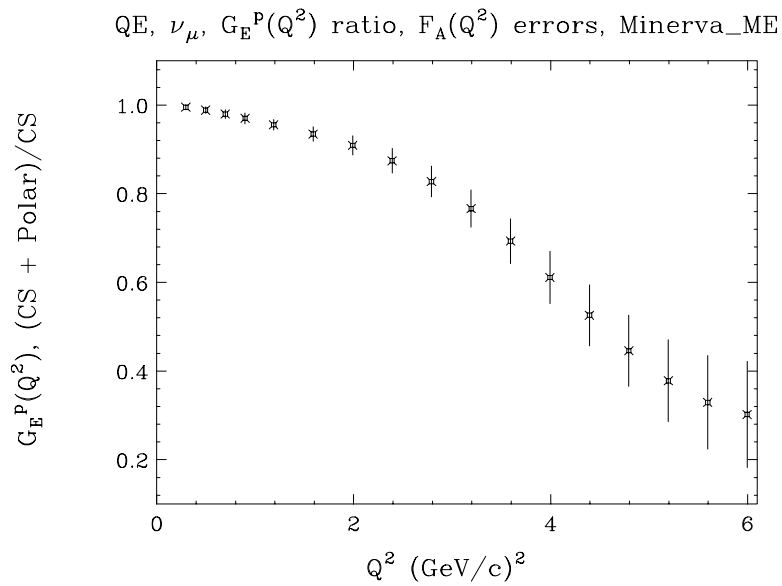
QE, ν_μ, $G_E{}^P(Q^2)$ ratio, $F_A(Q^2)$ errors, Minerva_ME

Figure 24: (a) Neutrino, (b) Antineutrino. The extracted ratio and error in F_A/F_A(Dipole) under the assumptions that this ratio is described by the ratio of G_E^p(Cross-Section)$/G_E^p$(dipole), which was the the accepted result for G_E^p before the new polarization transfer measurement. Note a ratio of 1.0 is expected if the axial form factor is described exactly by the dipole form. This corresponds to a total of the currently planned 4 years of running in the Low Energy Beam Configuration.
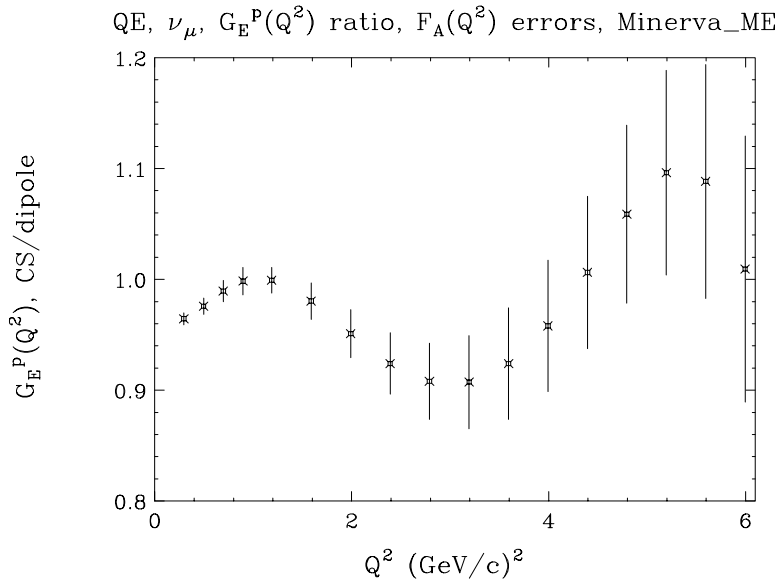
MINERvA active Cargon target under the assumption that F_A is described by the dipole form factor with M_A of 1 GeV. We use the various measurements of of G_E^p to illustrate the values and the errors on possible outcomes of MINERvA. Figure 22 show the extracted ratio and error in F_A/F_A(Dipole) under the assumptions that this ratio is described by the ratio of G_E^p(Cross-Section+POLARIZATION)$/G_E^p$(Dipole) (which is the currently assumed form factor for G_E^p in the BBA2003 parametrization). Figure 23 show the extracted ratio and error in F_A/F_A(Dipole) under the assumptions that this ratio is described by the ratio of G_E^p(Cross-Section+POLARIZATION)$/G_E^p$(Cross-Section). Figure 24 show the extracted ratio and error in F_A/F_A(Dipole) under the assumptions that this ratio is described by the ratio of G_E^p(Cross-Section)$/G_E^p$(dipole), which was the the accepted result for G_E^p before the new polarization transfer measurement. Note a ratio of 1.0 is expected if the axial form factor is described exactly by the dipole form.

5   Appendix D: An Introduction to Nuclear Effects

5.1   Plane Wave Impulse Approximation (PWIA)

A. Free protons

Although we plan to use much more sophisticated models in our analysis (in collaboration with the Ghent nuclear theoryh group), it is instructive to describe the use of the Fermi Gas model as an example of a model in which nuclear parameters are extracted from electron scattering data and applied to neutrino scattering experiments. Here we describe an treatment of Bodek and Ritchie, and also add the effect of the nuclear binding potential ϵ as described in Moniz. [30]. Before we discuss the kinematics of the scattering from an off-shell nucleon in a deuterium or heavy target nucleus, we consider the case of scattering from a free proton. We take the case of electron scattering to represent the general lepton-nucleon scattering at high energies. The kinematics of the scattering from a free proton of mass M_p is shown in Figure 25(a). The incident electron energy is E_0 and the final scattering energy in the laboratory system is E'. The scattering angle in the laboratory is defined as θ. The four-momentum transfer to the target proton is $q = (\vec{q}_3, q_0)$. We define the following variables in terms of laboratory energies and angles. The square of the invariant four-momentum transfer q is

$$q^2 = q_0^2 - \vec{q}_3^2 = -4E_0 E' \sin^2 \frac{\theta}{2} = -Q^2 \ .$$

The square of the initial target proton four-momentum P_i is

$$P_i^2 = M_p^2 \ .$$

The square of the final-state proton momentum P_f (which is equal to the final-

state invariant mass) is

$$
\begin{aligned}
P_f^2 &= W^2 = (P_i + q)^2 = P_i^2 + 2P_i \cdot q + q^2 \\
&= M_p^2 + 2M\nu - Q^2 \ ,
\end{aligned}
$$

where $\nu = E_0 - E' = q_0$ (in the laboratory system) and $x = Q^2/2q \cdot P_i = Q^2/2M_p\nu$.
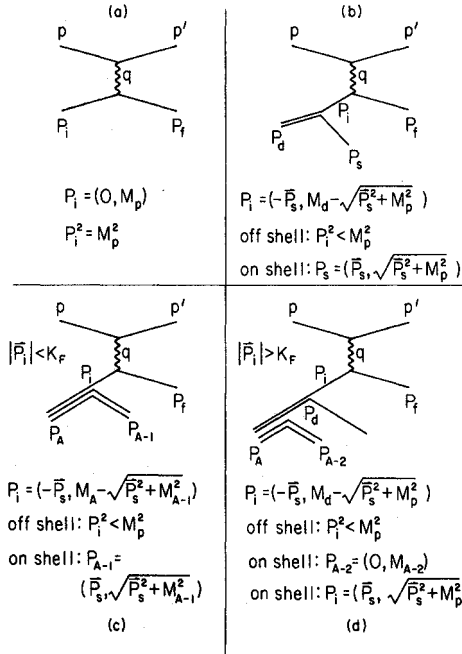

Figure 25: Kinematics for on-shell and off-shell scattering and scattering from off-shell nucleons in deuterium and nuclei. (a) Free nucleons. (b) A nucleon bound in the deuteron. (c) A nucleon with momentum $|\vec{P_i}| < K_F$ in a heavy nucleus of atomic weight A. (d) A nucleon bound in a heavy nucleus having momentum $|\vec{P}| > K_F$ due to an interaction with another nucleon. See text for details.

B. Scattering from an off-shell nucleon in the deuteron

In the impulse approximation, the spectator nucleon in the deuteron is free and is on the mass shell. It is totally unaffected by the interaction. The interacting nucleon with momentum P_i must be of the mass shell in order to conserve energy and momentum in the scattering process. The kinematics is shown in Figure 25(b). The Fermi motion does not change Q^2 but it does change the final-state invariant mass W and the quantity $P_i \cdot q$. Because the interacting nucleon is off the mass shell, its effective mass is less than the mass of the proton

29

and is a function of its momentum. The on-shell spectator has momentum $\vec{P}_s$ and on-shell energy $E_s = (\vec{P}_s^2 + M_p^2)^{1/2}$. The off-shell interacting proton has momentum $-\vec{P}_s$ and off-shell energy in the laboratory $E_i = M_d - E_s$, where M_d is the mass of the deuteron, i.e.,

$$\vec{P} = \vec{P}_i = -\vec{P}_s \quad \text{and} \quad E_i = M_d - (P_s^2 + M_p^2)^{1/2} \ .$$

After the scattering the invariant mass of the final state (neglecting the free spectator) is

$$
\begin{aligned}
P_f^2 &= W'^2 = (P_i + q)^2 = P_i^2 + 2P_i \cdot q - Q^2 \ , \\
W'^2 &= (E_i^2 - \vec{P}_s^2) + 2E_i\nu - 2P_3|\vec{q}_3| - Q^2 \ ,
\end{aligned}
$$

where P_3 is the momentum along the direction of the $\vec{q}_3$ vector.

C. Scattering from an off-shell nucleon in the nucleus $(P < K_F)$

For momenta less than the Fermi momenta K_F, the nucleon interacts with the average potential of all the nucleons in the nucleus of atomic weight A. Therefore, in the impulse approximation, the interacting nucleon has momentum P_i which is balanced by a excited recoiling nucleus with $A - 1$ nucleons and momentum $P_{A-1} = -P_i$. The interacting nucleon is off the mass shell, and the recoiling excited $A - 1$ nucleus is on the mass shell. After the collision, the recoiling nucleus remains in its excited state, M_{A-1}^* and all the particles are on the mass shell [see Figure 25(c)]. In the laboratory system we have

$$\vec{P} = \vec{P}_i = -\vec{P}_s \,, \quad E_i = (\vec{P}^2 + M_p^2)^{1/2} - \epsilon \ ,$$

where ϵ is the effective depth of average nucleon potential energy in GeV (e.g. 25 MeV for Carbon) and

$$W'^2 = (E_i^2 - \vec{P}_2^2) + 2E_i\nu - 2P_3|\vec{q}| - q^2 \ .$$

This process leaves behind an $A-1$ nucleus in an excited state M_{A-1}^*, which does not need to be calculated, but varies with $\vec{P}$ such that the following equation also holds

$$(\vec{P}_s^2 + M_{A-1}^{*2})^{1/2} = M_A - E_i \ ,$$

D. Scattering from an off-shell nucleon in the nucleus $(P \gg K_F)$

In the simple Fermi-gas model the nucleons cannot have momenta greater than the Fermi momentum K_F. However, such high momenta can come from the interaction between individual nucleons through their hard-core potential. In the case where the nucleon has acquired its high momentum by interacting with another single nucleon, one may assume that a single nucleon is recoiling against it. This case can be treated as having a quasideuteron in the nucleus with a excited spectator nucleus of $A - 2$ nucleons which is at rest in the laboratory system. If we neglect the excitation energy of the spectator nucleus, the kinematics [shown in Figure 25(d)] are the same as the scattering from a nucleon
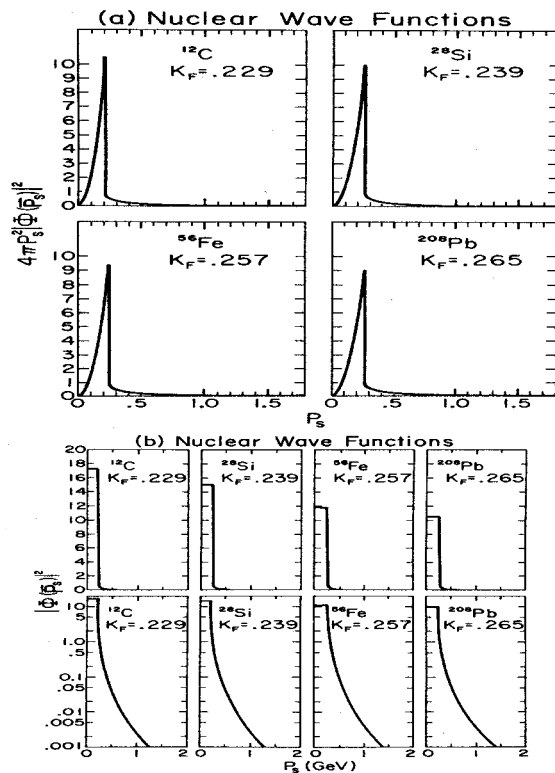
Figure 26: Fermi Gas wave functions, with and without a quasideuton tail. These momentum distributions used in the calculations of Bodek and Ritchie for ^{12}C, ^{28}Si, ^{56}Fe and ^{208}Pb. (a) $4\pi|\vec{P}|^2\phi(\vec{P})|^2$. (b) $|\phi(\vec{P})|^2$

bound in the deuteron. However (within this rather simplified model for the high mometum tails) one can also correct for the fact that the $A-2$ nucleons are on average in an excited state because two nucleons each with average binding potential energy ϵ were removed:

$$\vec{P} = \vec{P}_i = -\vec{P}_s \quad \text{and} \quad E_i = M_d - (P_s^2 + M_p^2)^{1/2} - 2\epsilon \ .$$

E. Nuclear Momentum Distributions

If the Fermi-Gas model is to used to predict neutrino cross sections on nuclei, it is best to use Fermi-gas momentum distributions that are obtained from fits to quasielastic electron-scattering data from heavy nuclei. In the Fermi-gas model the momentum distribution is constant up to the maximum Fermi momentum K_F and is zero above K_F. One can also add a high-momentum tail to the momentum distribution (according to Moniz [31]) which is based on calculations of nucleon-nucleon correlations in nuclear matter. The normalized momentum
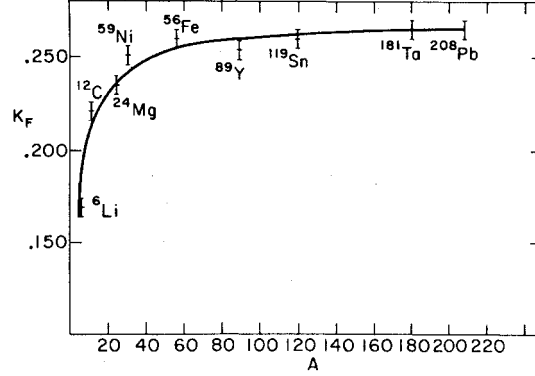
31

Figure 27: Fits to the effective K_f (within a Fermi-gas model) for various nuclei from Moniz. [30] used by Bodek and Ritchie.

distributions with tail (e.g. if we use this model up to $P_{max} = 0.75$ GeV) are:

$$|\phi(\vec{P})|^2 = \frac{1}{C}\left[1 - 6\left(\frac{K_F a}{\pi}\right)^2\right]$$

$$\text{for } 0 < |\vec{P}| < K_F \ ,$$

$$|\phi(\vec{P})|^2 = \frac{1}{C}\left[2R\left(\frac{K_F a}{\pi}\right)^2\left(\frac{K_F}{P}\right)^4\right]$$

$$\text{for } K_F < |\vec{P}| < P_{max} \ ,$$

$$|\phi(\vec{P})|^2 = 0 \text{ for } |\vec{P}| > P_{max}$$

with $a = 2$ (GeV/c)$^{-1}$, $C = \frac{4}{3}\pi K_F^3$, and $R = 1/[1 - K_F/(P_{max}]$. These momentum distributions satisfy the normalization

$$\int_0^{P_{max}} |\phi(\vec{P})|^2 4\pi P^2 dp = 1.0 \ .$$

The difference in the momentum distributions for protons and neutrons is taken into account as follows:

$$K_F^p = K_F\left(\frac{2Z}{A}\right)^{1/3} \ ,$$

$$K_F^n = K_F\left(\frac{2N}{A}\right)^{1/3} \ ,$$

where $A = A + N$ is the atomic weight. Z is the number of protons, and N is the number of neutrons. For an isoscalar target $Z = N = A/2$ and

32

$K_F^p = K_F^n = K_F$. The momentum distribution for carbon (^{12}C), silicon (^{28}Si), iron (^{56}Fe), and lead (^{208}Pb) are shown in linear and logarithmic scales in Figures 26(b) and 25(a). The Fermi momenta that are shown are 0.221 GeV/c for ^{12}C, 0.257 GeV/c for ^{56}Fe, and 0.265 GeV/c for ^{208}Pb. These are from fits by Moniz, which also extracted ϵ values of 25, 36 and 44 MeV, respectively.

Although in the original paper of Bodek and Ritchie the form for the additional tail was used up to momenta of P_{max}=4 GeV/c, it is probably better to use this tail only up to P_{max}=0.75 GeV/c. For a calculation which does not include the additional tail, the expressions are:

$$|\phi(\vec{P})|^2 = \frac{1}{C} \text{ for } 0 < |\vec{P}| < K_F ,$$

$$|\phi(\vec{P})|^2 = 0 \text{ for } |\vec{P}| > K_F$$

F. Nuclear Spectral functions

The above Fermi Motion model, with or without tail is relatively easy to use in Monte Carlo simulations. The Fermi gas model is a special case of a spectral function with specific approximation to the momentum distribution and nucleon removal energy. More refined models use electron scattering data to extract spectral functions which give the correlated information between the momentum of the nucleon and the nucleon removal potential binding for the different shell-model nucleons in different energy levels in the nucleus.

However, it is important to realize that as long as the parameters within a given nuclear model are empirically fit and extracted from electron scattering data, these models can be used rather reliably to predict the corresponding nuclear effects in neutrino scattering (especially for vector scattering).

References

[1] Y. Fukada *et al.*, Phys. Rev. Lett. 81 (1998) 1562.

[2] H. Budd, A. Bodek and J. Arrington, hep-ex/0308005 (published in Proceedings of NuInt02 - this conference, Nucl, Phys. B, Proceedings Suppl); A. Bodek, H. Budd and J. Arrington, hep-ex/0309024 (to be published in Proceedings of CIPANP2003, New York City, NY 2003.

[3] C.H. Llewellyn Smith, Phys. Rep. 3C (1972).

[4] S. Adler, Phys. Rev. **143**, 1144 (1966); F. Gillman, Phys. Rev. **167**, 1365 (1968).

[5] D. Drechsel, B. Pasquini, M. Vanderhaeghen, hep-ph/0212123.

[6] V. Bernard, L. Elouadrhiri, U.G. Meissner, J.Phys.G28 (2002), hep-ph/0107088.

[7] J. Arrington, nucl-ex/0305009.

[8] E. J. Brash*et al.*Phys., Rev. C, 65, 051001(R)

[9] M. Paschos, private communication

[10] M. Strikman, private communication

[11] M. K. Jones *et al.*, Phys. Rev. Lett, 84, (2000) 1398 ; O. Gayou *et al.*, Phys. Rev. Lett, 88 (2002) 092301.

[12] A.F. Krutov, V.E. Troitsky, Eur. Phys. J. A16 (2003) 285, hep-ph/0202183.

[13] S. Glaster *et al.*, Nucl. Phys. B32 (1971) 221.

[14] N.J. Baker *et al.*, Phys. Rev. D23 (1981) 2499.

[15] S.J. Barish *et al.*, Phys. Rev. D16 (1977) 3103.

[16] K.L. Miller *et al.*, Phys. Rev. D26 (1982) 537.

[17] T. Kitagaki *et al.*, Phys. Rev. D26 (1983) 436.

[18] T. Kitagaki *et al.*, Phys. Rev. Lett. 49 (1982) 98.

[19] M.G. Olsson, E.T. Osyporeski and E.H. Monsay, Phys. Rev. D17 (1978) 2938.

[20] S.K. Singh, Nucl. Phys. B36 (1972) 419.

[21] Particle Data Group, Eur. Phys. J C15 (2000) 196.

[22] W.A. Mann *et al.*, Phys. Rev. Lett. 31 (1973) 844.

[23] J. Brunner *et al.*, Z. Phys. C45 (1990) 551.

[24] M. Pohl *et al.*, Lett. Nuovo Cimento 26 (1979) 332.

[25] L.B. Auerbach *et al.*, Phys. Rev. C66 (2002) 015501.

[26] S.V. Belikov *et al.*, Z. Phys. A320 (1985) 625.

[27] S. Bonetti *et al.*, Nuovo Cimento 38 (1977) 260.

[28] N. Armenise *et al.*, Nucl. Phys. B152 (1979) 365.

[29] G. Zeller, private communication.

[30] R.A. Smith and E.J. Moniz, Nucl. Phys. B43 (1972) 605; E. J. Moniz *et al.*, Phys. Rev. Lett. 26. 445 (1971); E. J. Moniz, Phys. Rev. 184, 1154 (1969).

[31] E. J. Moniz, private communication; W. Czyz and K. Gottfried, Nucl. Phys. **21**, 676 (1961); W. Czyz and K. Gottfried, Ann. Phys. NY **21**, 47 (1963);K. Gottfried, *ibid*, **21**, 29 (1963).

[32] D. Casper, Nucl. Phys. Proc. Suppl. 112 (2002) 161.

[33] K. Tsushima, Hungchong Kim, K. Saito, nucl-th[0307013].

[34] A. Bodek and J. L. Ritchie, Phys. Rev. D23 (1981) 1070; ibid Phys. Rev. D24 (1981) 1400.

[35] Ghent Theory group in Belgium (Jan Ryckebusch, jan@inwpent5.UGent.be)

(http://inwpent5.ugent.be/papers/santorini.pdf\end{verbatim

\bibitem{mark1} M. Strikman, private communication. See also talk by
 Rholf Ent, these proceedings;
 L. Lapikas, et al Phys.Rev.C61:064325,2000 (nucl-ex/9905009);
 L. Frankfurt, M. Strikman and M. Zhalov, Phys.Lett.B503:73-80,2001
(hep-ph/0011088)

\bibitem{e94110} JLab hydrogen experiment 94-110, C.E. Keppel spokesperson
\begin{verbatim}(http://www.jlab.org/exp_prog/proposals/94/PR94-110.pdf)

[36] JLab deuterium experiment 02-109, C.E. Keppel, M. E. Christy, spokespersons

(http://www.jlab.org/exp_prog/proposals/02/PR02-109.ps)

[37] JLab experiment 99-118 on the nuclear dependence of R at low Q^2, A. Brull, C.E. Keppel spokespersons

[38] Jlab Proposal PR03-110 on Nuclear Targets (C, Fe), A. Bodek and C. E. Keppel, Spokespersons; proposed to be run at the same time as deuterium experiment E02-109.

[39] U. K. Yang and A. Bodek, Phys. Rev. Lett. **82**, 2467 (1999).

[40] U. K. Yang and A. Bodek, Eur. Phys. J. C**13**, 241 (2000).

[41] U. K. Yang, Ph.D. thesis, Univ. of Rochester, UR-1583 (2001).

[42] L. W. Whitlow *et al.* (SLAC-MIT) , Phys. Lett. B**282**, 433 (1995); A. C. Benvenuti *et al.* (BCDMS) , Phys. Lett. B**237**, 592 (1990);

M. Arneodo *et al.* (NMC) , Nucl. Phys. B**483**, 3 (1997).

[43] H. Georgi and H. D. Politzer, Phys. Rev. D**14**, 1829 (1976); R. Barbieri *et al.*, Phys. Lett. B**64**, 171 (1976), and Nucl. Phys. B**117**, 50 (1976); J. Pestieau and J. Urias, Phys.Rev.D**8**, 1552 (1973)

[44] A.L. Kataev *et al.*, Phys. Lett. B**417**, 374 (1998), and also hep-ph/0106221; J. Bluemlein and A. Tkabladze, Nucl. Phys. B**553**, 427 (1999).

[45] A. Bodek and U. K. Yang, `hep-ex/0203009`, (NuInt01 proceedings) Nucl.Phys.Proc.Suppl.112:70-76,2002.

[46] A. Bodek, U. K. Yang, `hep-ex/0210024`, (NuFact'02 proceedings) J. Phys. G. Nucl. Part. Phys.,**29**, 1899 (2003); A. Bodek and U. K. Yang, `hep-ex/0308007`, (published in Proceedings of NuInt02 - this conference, Nucl, Phys. B, Proceedings Suppl); A. Bodek and U. K. Yang, `hep-ex/0301036` (proceedings of the Mexico Particle Physics summer school 2002).

[47] A. Bodek *et al.*, Phys. Rev. D**20**, 1471 (1979).

[48] A. Donnachie and P. V. Landshoff, Z. Phys. C **61**, 139 (1994); B. T. Fleming *et al.*(CCFR), Phys. Rev. Lett. **86**, 5430 (2001). Note that QCD evolution is completely neglected in these earlier analyses of very low Q^2 data. In contrast we include QCD evolution, low Q^2 non-perturbative effects target mass and higher twist terms in our fits.

[49] S. Stein *et al.*, Phys. Rev. D**12**, 1884 (1975); K. Gottfried, Phys. Rev. Lett. **18**, 1174 (1967).

[50] U. K. Yang *et al.*(CCFR), Phys. Rev. Lett. **87**, 251802 (2001).

[51] E. D. Bloom and F. J. Gilman, Phys. Rev. Lett. **25**, 1140 (1970).

[52] C. S. Armstrong *et al.*, Phys. Rev. D**63**, 094008 (2001) (www.jlab.org/resdata/). [also Phys. Rev. Lett. **85** , 1182 (2000); Phys. Rev. Lett. **85**, 1186 (2000); Phys. Rev. D **62**, 073008 (2000); Phys Rev. D **64**, 038302 (2001); Phys. Rev. C **64**, 014602 (2001); C. Keppel, Proc. of the Workshop on Exclusive Processes at High P_T, Newport News, VA, May (2002).]

[53] D. Rein and L. M. Sehgal, Annals Phys. **133** 79 (1981) and D. Rein, Z. Phys. C. 35, 43 (1987) (neutrino production); R. P. Feynman, M. Kislinger, and F. Ravndal, Phys. Rev. D 3, 2706 (1971); FKR: F. Ravndal, Phys. Rev. D4, 1466 (1971) (electroproduction); Kneis, Moorhouse, Oberlack, Phys. Rev. D9, 2680 (1974) (photoproduction); R. Belusevic and D. Rein, Phys. Rev. D **46**, 3747 (1992) (neutrino coherent processes on nuclei).,

[54] K. Sato and T. S. H. Lee nucl-th/0303050 (2003) (neutrino production); T. Sato, D. Uno and T.S. Lee, Phys. Rev. C63.-55201 (2001) (electroproduction)

[55] S. Kretzer and M.H. Reno, hep-ph/0208187

[56] Badelek and Kwiecinski, Nucl. Phys. **B370**, 278 (1992).